

# Elongation of Triblock Copolymer Melt: Elongation Flow Opto-Rheometry and Small-Angle X-ray Scattering Study

Yuka Kobori,<sup>†,§</sup> Yong Ku Kwon,<sup>\*,‡</sup> Masami Okamoto,<sup>\*,†</sup> and Tadao Kotaka<sup>†</sup>

*Advanced Polymeric Materials Engineering, Graduate School of Engineering, Toyota Technological Institute, Hisakata 2-12-1, Tempaku, Nagoya 468-8511, Japan, and Department of Polymer Science and Engineering, Inha University, 253 Yonghyun-Dong, Nam-Gu, Incheon 402-751, Korea*

*Received March 29, 2002*

**ABSTRACT:** The elongational flow-induced morphological change of a triblock copolymer melt of polystyrene-*b*-poly(ethylene butylene)-*b*-polystyrene (SEBS) with polystyrene (PS) weight fraction of 30% has been investigated using elongational flow opto-rheometry (EFOR) and small-angle X-ray scattering (SAXS). The alignment of the PS cylindrical domains in a preferred direction is achieved by roll processing at 200 °C. In the EFOR measurement, the uniaxial elongation with a Hencky strain rate,  $\dot{\epsilon}_0$ , of 0.01 s<sup>-1</sup> is applied at 180 °C in the direction either parallel (case 1 elongation) or perpendicular (case 2 elongation) to the cylinder axis. Transient elongational viscosity,  $\eta(\dot{\epsilon}_0; t)$ , measured during the case 1 elongation exhibits an initial increase, followed by a gradual decrease to almost a steady state before rupture. One measured during the case 2 elongation shows three different regions with elongation time: an initial increase followed by a gradual decrease and a final, rapid increase. The SAXS measurement on the elongated films demonstrates that the alignment of the cylindrical domains persists during the case 1 elongation, whereas the cylindrical domains are rotated by 90° to be aligned parallel to the elongation direction during the case 2 elongation, indicating that the final orientation of the cylinders is not determined by the initial alignment of the domain, but by the Hencky strain rate and the tensile stress level applied on the specimen.

## Introduction

The elongational flow behavior of heterogeneous polymer melts, for example, block copolymers and polymer blends, is complicated due to the structural evolution of phase morphology as well as the nonlinear elongational flow response of component polymers.<sup>1–5</sup> Nanophase-separated block copolymers are known to display various domain structures, depending on the chemistry and composition of component block segments.<sup>6</sup> The aggregation of domains forms a grain on a micrometer scale, and both domain and grain structure affect their macroscopic mechanical and rheological properties. Our previous studies on polystyrene-*b*-poly(ethylene butylene)-*b*-polystyrene-*b*-poly(ethylene butylene) (SEBSEB) tetrablock and polystyrene-*b*-poly(ethylene butylene)-*b*-polystyrene (SEBS) triblock copolymer demonstrated that their birefringences,  $\Delta n(\dot{\epsilon}_0; t)$ , and stress–optical coefficients,  $C(\dot{\epsilon}_0; t)$ , measured during elongation deviated positively over the values typically observed in the elongation of homopolymer melts.<sup>5</sup> Such behavior was attributed to the form birefringence of the phase-separated domain morphology developed in elongational-flow field. It was also reported that the elongated morphology of these block copolymers varied with the elongation conditions such as strain rate and temperature.

In past decades, the deformation behavior of block copolymers in shear-flow field has been investigated in great detail. It has been reported that a large-amplitude oscillatory shear induces the alignment of the domains

of diblock copolymers either parallel or perpendicular to the shearing direction, depending on shearing temperature and molecular weight of component blocks.<sup>7–13</sup> Polis and Winey<sup>8</sup> demonstrated the continuous rotation process of the lamellae of a diblock copolymer of polystyrene-*b*-poly(ethylene propylene) under a large-amplitude oscillatory shear and explained the formation of kink bands in the sheared lamellae by the layer rotation mechanism.

Elongation of block copolymers has attracted recent research interest due to their interesting morphological responses at large deformation.<sup>4,15–20</sup> Most studies reported to date have been carried out below the  $T_g$  of the rigid block and described the deformation initiated in localized regions or at defects. Pakula et al.<sup>18</sup> reported that polystyrene-*b*-polybutadiene-*b*-polystyrene (SBS) triblock copolymer with cylindrical domains underwent fragmentation and reorientation during elongation and displayed a deformed morphology. The long axis of the cylindrical domains was inclined to the elongation direction at a stretching ratio of approximately 7. Regardless of the initial orientation of the cylindrical domains, the final deformed morphologies of all the tested specimens were almost the same, indicating that the amount of elongation applied was significant to determine the deformation behavior of SBS. Most studies on the elongation of block copolymers have focused on the deformation of the lamellar morphology of triblock copolymers subjected in large strains at room temperature and demonstrate that the deformed morphology varies with several factors such as initial orientation of domains, amount of strain applied, and domain orientation, relative to the stretching direction.

Our previous studies on SEBS and SEBSEB, carried out at high temperatures between the  $T_g$  of polystyrene (PS) and their order–disorder transition temperatures ( $T_{ODT}$ 's), also suggested that the elongated morphologies

<sup>†</sup> Toyota Technological Institute.

<sup>‡</sup> Inha University.

<sup>§</sup> Current address: Institute of Physical and Chemical Research, Hirosawa 2-1, Wako-shi, Saitama 351-0198, Japan.

\* To whom correspondence should be sent. E-mail: okamoto@toyota-ti.ac.jp or ykkwon@inha.ac.kr.

of the cylindrical and spherical domains were controlled by the applied strain rate. It was also reported that fast elongation resulted in a tilted phase, whereas slow elongation caused the parallel alignment of the cylindrical domain.<sup>5</sup> The elongational viscosities,  $\eta_E(\dot{\epsilon}_0; t)$ , enormously increased at low strain rates (strain-induced hardening), indicating that both molecules and domains were highly aligned to the stretching direction.

In the present study, we continue to investigate the elongational deformation behavior of the SEBS triblock copolymer with cylindrical microdomains much above  $T_g$  of mechanically rigid PS blocks by using elongational flow opto-rheometry (EFOR) and small-angle X-ray scattering (SAXS). This study attempts to provide the detailed information on the structural and morphological evolution of the cylindrical morphology subjected in elongational flow field at high temperatures.

Our EFOR, equipped with a high-precision birefringence optics, enables us to measure simultaneously transient tensile stress  $\sigma(\dot{\epsilon}_0; t)$  and birefringence  $\Delta n(\dot{\epsilon}_0; t)$  as a function of time and Hencky strain rate  $\dot{\epsilon}_0$  in the range  $0.001-1.0 \text{ s}^{-1}$ .<sup>21</sup> The attainable maximum Hencky strain  $\epsilon_{H, \max}$  ( $\equiv \ln \lambda_{\max}$ ) can reach as much as 7, which corresponds to the maximum stretch ratio  $\lambda_{\max}$  ( $= L_f/L_0$  where  $L_f$  and  $L_0$  represent the final and original length of sample, respectively) of approximately 1100, as long as the specimen is not ruptured during elongation. The EFOR measurement in the present study is performed on SEBS with the preferred orientation of polystyrene cylinders during uniaxial elongation with  $\dot{\epsilon}_0 = 0.01 \text{ s}^{-1}$  at the temperatures between the  $T_g$  of the PS block and the reported  $T_{\text{ODT}}$  of SEBS. Our results provide the detailed information on the cylinder rotation of triblock copolymers subjected in elongational flow.

## Experimental Section

**Materials.** The SEBS triblock copolymer with a PS weight fraction of 30% (corresponding volume fraction of 25%) (Asahi Chemical Co.) was used in this study. The molecular weight of the polymer was determined by gel permeation chromatography (GPC) using PS elution standards: a weight-average molecular weight,  $M_w$ , was  $92.6 \text{ kg mol}^{-1}$  and a polydispersity index was 1.17. The  $T_{\text{ODT}}$  of SEBS could not be detected up to  $300 \text{ }^\circ\text{C}$  in our rheological measurement and has been estimated to be greater than  $300 \text{ }^\circ\text{C}$ . The block sequence of the polymer was estimated to be 13.9–64.8–13.9 in units of  $\text{kg mol}^{-1}$ .

**Sample Preparation.** The compressed films of as-received SEBS pellets were prepared by molding at  $200 \text{ }^\circ\text{C}$ . The alignment of the cylinder domains was achieved by uniaxial roll processing by counter-rotating two rollers at  $200 \text{ }^\circ\text{C}$  for about 10 min. They were transferred to another hot press kept at ambient temperature and pressure without applying load and allowed to be cooled by circulating chilled water into the jacket of a hot press.

Specimens for the EFOR measurement had dimensions of about  $60.0$  (length)  $\times$   $7.0$  (width)  $\times$   $2.5$  (thickness)  $\text{mm}^3$ , prepared by cutting a roll-processed sheet in the direction either parallel or perpendicular to the rolling direction. The initial morphology of the unelongated samples was checked by SAXS prior to the EFOR measurement. Whether the cylindrical phase of a sample strip was globally aligned was confirmed by monitoring the orientation of the cylindrical domain at different positions in a sample strip. The elongated samples collected at various stages of elongation were quenched into ice water to freeze the deformed morphologies and kept at room temperature prior to SAXS measurements. Whether the undesirable relaxation or change in the cylinder orientation occurred between the EFOR and SAXS measurement was also checked by collecting the SAXS data of the sample just after the EFOR and during the SAXS measurement.

**SAXS Apparatus.** The measurements were carried out in our SAXS apparatus consisting of a 6 kW rotating-anode X-ray generator (M06X<sup>CE</sup>, MAC Science Co. Ltd.) with Cu K $\alpha$  radiation (wavelength,  $\lambda_{\text{scat}} = 0.154 \text{ nm}$ ), operated at 50 kV and 24 mA. It includes a Ge monochromator, point-focusing optics, and a vacuum chamber for the incident beam path and scattered beam path and a two-dimensional imaging plate detector. The distance between the sample and detector was set at 700 mm. The correction for slit-width smearing was not needed due to the fine, point-focusing cross section ( $0.1 \text{ mm} \times 1 \text{ mm}$ ) of the primary X-ray beam used in this study.

Two-dimensional SAXS patterns of the specimens collected during various stages of elongation were taken at room temperature. The data on the angular dependence of the SAXS intensity were obtained by scanning through the peak intensities on the observed patterns and then digitally saved for further analysis. Another set of the scanned data was also collected by scanning along the azimuthal direction of the main intense peak. The data in the range of  $0 < q$  ( $= 4\pi \sin \theta/\lambda$  where  $2\theta$  is a scattering angle) ( $\text{nm}^{-1}$ )  $\leq 0.4$  and  $0.4 < q$  ( $\text{nm}^{-1}$ )  $\leq 1.5$  were measured separately with different X-ray exposure times to achieve adequate signal-to-noise ratios at higher  $q$  values.

**EFOR Measurement.** The elongational flow opto-rheometer employed in our study was a combination of a Meissner's new elongational rheometer of gas-cushion type commercialized as Rheometrics Melt Elongational rheometer (RME: Rheometrics Scientific Co.) which was described elsewhere.<sup>22</sup> In the measurement, the Hencky strain rate  $\dot{\epsilon}$  is defined under assumption of affine deformation described below:

$$\dot{\epsilon} = \dot{\epsilon}_0 h(t) \quad (1)$$

where  $\dot{\epsilon}_0 = (1/L_0)(dL_0/dt) = [1/L(t)][dL(t)/dt]$  [ $L_0$  and  $L(t)$  ( $= L_0 \exp \dot{\epsilon}_0 t$ ) represents the initial and elongated dimension at time  $t$ , and  $h(t)$  is a unit step function: 1 for  $t \geq 0$  and 0 for  $t < 0$ ]. Assuming no volume change of a sample during elongation, i.e.,  $A_0 L_0 = A(t) L(t)$  where  $A_0$  and  $A(t)$  [ $= A_0 \exp(-\dot{\epsilon}_0 t)$ ] are the initial and elongated cross-sectional area at time  $t$ , then the Hencky strain  $\epsilon(t)$  is expressed as

$$\epsilon(t) (\equiv \dot{\epsilon}_0 t) = \ln \left( \frac{L(t)}{L_0} \right) = \ln \lambda(t) \quad \text{for } t \geq 0 \quad (2)$$

where  $\lambda(t)$  [ $= L(t)/L_0$ ] denotes the stretching ratio at time  $t$ . In each run, the tensile force  $F(\dot{\epsilon}_0; t)$  at  $t$  is converted to the tensile stress  $\sigma(\dot{\epsilon}_0; t)$  by dividing by the cross-sectional area,  $A(t)$ , of the sample at  $t$ . The elongational viscosity is given by

$$\eta_E(\dot{\epsilon}_0; t) = \frac{\sigma(\dot{\epsilon}_0; t)}{\dot{\epsilon}_0} \quad (3)$$

In our measurement, a sample strip was clamped between two metal belt conveyers at a fixed distance  $L_0$  and annealed at  $180 \text{ }^\circ\text{C}$  for 120 s to remove mechanical and thermal history on the samples acquired prior to elongation. The measurement was usually carried out at  $180 \text{ }^\circ\text{C}$  with a Hencky strain rate of  $0.01 \text{ s}^{-1}$ . The data measured at different temperatures and strain rates will be reported in a separate publication.<sup>23</sup> For convenience, we denote the elongation in the direction parallel to the cylinder axis as the case 1 elongation and that perpendicular to the cylinder axis as the case 2 elongation.

The tensile force and retardation were simultaneously measured during measurement. The estimation of the birefringence  $\Delta n(\dot{\epsilon}_0; t)$  requires the thickness of the specimen at time  $t$ . Assuming no volume change of the specimen during elongation, we estimated both cross-sectional area and thickness from the initial dimensions measured prior to elongation at the ambient temperature. Then, the specific volume,  $\bar{v}_{\text{SEBS}}$ , of SEBS was assumed to be additive of those of the component homopolymers as shown below:

$$\bar{v}_{\text{SEBS}} = w_{\text{PS}} \bar{v}_{\text{PS}}(T) + w_{\text{PEB}} \bar{v}_{\text{PEB}}(T) \quad (4)$$

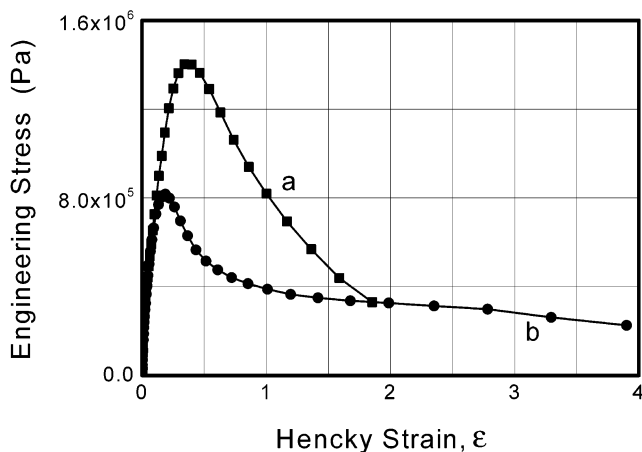


**Figure 1.** Engineering stress and strain curves of the SEBS samples subjected in the (a) case 1 and (b) case 2 elongation.

where  $w_{PS}$  and  $w_{PEB}$  are weight fractions;  $\bar{v}_{PS}(T)$  and  $\bar{v}_{PEB}(T)$  are the specific volumes of the PS and PEB homopolymers as a function of temperature,  $T$ , which are adopted from the literature data<sup>24</sup> and the specific volume data of amorphous low-density polyethylene [=  $1.262 + 0.0009 \times (T - 125)$ ],<sup>25</sup> respectively. The difference between the intensities of one detector,  $S_p$  (+45° inclination to the stretching direction) and the other detector,  $S_s$  (-45° inclination to the stretching direction), was offset prior to the EFOR measurement, and the time evolution of the birefringence  $\Delta n(\dot{\epsilon}_0; t)$  was then determined. The details were described elsewhere.<sup>22</sup>

## Results

**Stress–Strain Curve.** Figure 1 shows the plots of engineering stress,  $\sigma(\dot{\epsilon}_0; t)$  [=  $F(\dot{\epsilon}_0; t)/A_0$ ] vs Hencky strain  $\epsilon(t)$  of (a) the case 1 and (b) the case 2 elongation at 180 °C with  $\dot{\epsilon}_0 = 0.01 \text{ s}^{-1}$ . The measurements were carried out at least three times for each experiment to achieve statistically significant averages. The data showed that the samples were ruptured near  $\epsilon \sim 1.8$  (after approximately 180 s) during the case 1 elongation, whereas they were highly elongated up to  $\epsilon \sim 3.9$  (after  $\sim 390$  s) in the case 2 elongation. The maximum yield stress and strain measured in the case 1 elongation were both greater than those in the case 2 elongation.

In the case 1 elongation, the PS and PEB domains are aligned parallel to the elongation direction. Because of the bridging midblock conformation of the PEB molecules, effective for stress transfer between mechanically rigid PS domains, the case 1 elongation exhibits the higher initial modulus and yield stress. In the case 2 elongation, on the other hand, the alternate arrangement of the PS and PEB domains to the stretching direction leads to the preferential elongation of the matrix PEB in the early stage of elongation, resulting in a lower initial modulus, yield stress, and yield strain value, as compared to one measured in the case 1 elongation.

**Elongational Viscosity.** Figure 2 shows the elongational viscosities,  $\eta_E(\dot{\epsilon}_0; t)$ , measured at 180 °C against elongation time  $t$  on a double-logarithmic scale during (a) the case 1 and (b) the case 2 elongation with  $\dot{\epsilon}_0 = 0.01 \text{ s}^{-1}$ . In the case 1 elongation shown in Figure 2a, the  $\eta_E(\dot{\epsilon}_0; t)$  increases continuously with  $t$  up to near  $\epsilon = 0.4$  and then remains almost constant for a while, followed by a slight decrease before rupture. Because of the parallel arrangement of the PS and PEB domains, the early elongation probably causes the orientation of the PS and PEB molecules in the disordered phase to

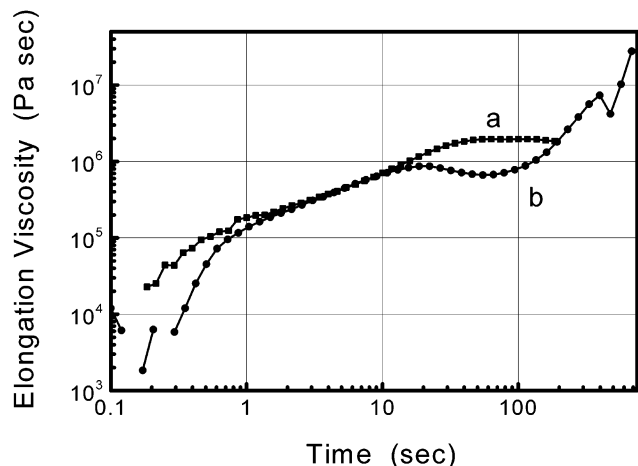


**Figure 2.** Plots of elongational viscosity vs time at 180 °C and with a strain rate of  $0.01 \text{ s}^{-1}$ : (a) case 1 and (b) case 2 elongation.

the stretching direction, which then leads to the initial increase of the  $\eta_E(\dot{\epsilon}_0; t)$  up to  $\epsilon = 0.4$ . The almost constant  $\eta_E(\dot{\epsilon}_0; t)$  value on further elongation for  $\epsilon > 0.4$  may be a result of the slipping of the domains and grains along the stretching direction. The slight decrease in the final stage of  $\eta_E(\dot{\epsilon}_0; t)$  just before rupture may be indicative of the strain-induced softening behavior, as described in our previous papers.<sup>5</sup>

In the case 2 elongation, the  $\eta_E(\dot{\epsilon}_0; t)$  data may be divided with  $t$  (or Hencky strain  $\epsilon$ ) into three regions: an initial increase up to  $\epsilon = 0.2$ , a decrease to almost the steady state in the range of  $0.2 < \epsilon \leq 0.7$  and a rapid final increase before rupture. In the perpendicular elongation, the measured  $\eta_E(\dot{\epsilon}_0; t)$  does not show a plateau region, revealing that the steady state is not observed. Because of the alternate arrangement of the PS and PEB domains to the stretching direction, the preferential deformation of the PEB matrix caused the initial, small  $\eta_E(\dot{\epsilon}_0; t)$ , compared to one measured in the case 1 elongation. On further elongation in the range of  $0.2 < \epsilon \leq 0.7$ , the stress on PEB molecules was transferred to the PS cylindrical domains to rearrange the domain and grain structure to the stretching direction, leading to a change in the observed  $\eta_E(\dot{\epsilon}_0; t)$ . In the final stage of elongation, the yielded domain structure experienced the further reorganization or realignment along the elongation direction, showing the further increase in  $\eta_E(\dot{\epsilon}_0; t)$ , indicative of strain-induced hardening behavior. The larger  $\eta_E(\dot{\epsilon}_0; t)$  values for the case 2 elongation compared to one measured in the case 1 elongation were probably due to a larger grain size with better orientation of the domain structure at large deformation in the case 2 elongation.

The scattered initial  $\eta_E(\dot{\epsilon}_0; t)$  in the beginning of both elongations were presumably due to the slight distortion of the sample geometry during equilibrating at 180 °C prior to measurement. The difference between two sets of  $\eta_E(\dot{\epsilon}_0; t)$  data in the first stage of elongation up to  $\epsilon = 0.2$  may result from different orientations of the cylinders in both cases. It was reported that the parallel and perpendicular orientation of the lamellae relative to the shearing direction exhibited different rheological responses in the beginning of deformation.<sup>8–13</sup>

**SAXS Results.** Figure 3a–d shows a series of the SAXS patterns of the unelongated and elongated samples subjected in the case 1 elongation, collected at (a) 0 s (unelongated), (b) 20 s ( $\epsilon = 0.2$ ,  $\lambda = 1.2$ ), (c) 90 s ( $\epsilon =$

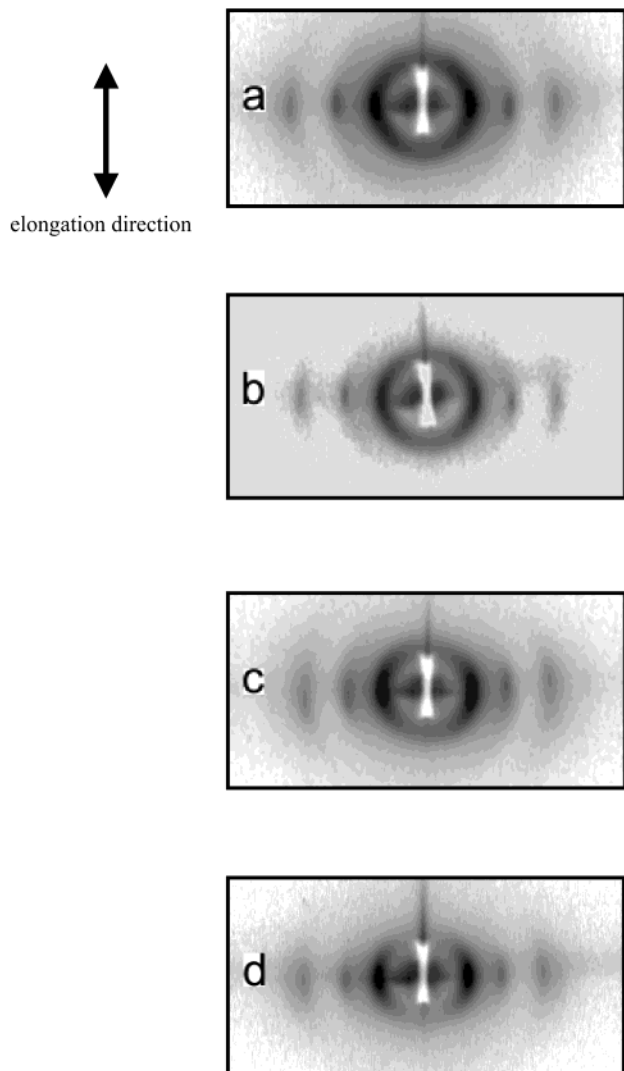


**Figure 3.** Two-dimensional SAXS patterns of the unelongated and elongated samples collected during the case 1 elongation at (a) 0 s (unelongated), (b) 20 s ( $\epsilon = 0.2$ ,  $\lambda = 1.2$ ), (c) 90 s ( $\epsilon = 0.9$ ,  $\lambda = 2.5$ ), and (d) 190 s ( $\epsilon = 1.9$ ,  $\lambda = 6.7$ ).

0.9,  $\lambda = 2.5$ ), and (d) 190 s ( $\epsilon = 1.9$ ,  $\lambda = 6.7$ ) during elongation. The corresponding one-dimensional SAXS scans of  $I(q)$  vs the scattering vector,  $q$ , were obtained by scanning through the peak intensities in Figure 3 and shown in Figure 4a–d. The data have been multiplied by a factor of  $10^3$  to avoid overlapping between data.

Figure 4a shows a series of equatorial X-ray peaks, confirming that the PS cylindrical axes of the unelongated sample were initially aligned along the stretching direction. The amorphous halo, overlapped with the most intense peak, was relatively intense, indicating that the disordered cylindrical phase coexisted with the ordered phase. In Figure 4a–d, we found an intense main peak at around  $q \approx 0.29 \text{ nm}^{-1}$  and additional higher-order peak maxima in the range of  $0.4 < q (\text{nm}^{-1}) \leq 1.0$ . They were approximately in the ratio of  $1:\sqrt{3}:\sqrt{7}$ , indicating that the cylinders are packed in a two-dimensional hexagonal lattice. The most intense peak was indexed as 100 hexagonal peak, and the additional peaks were assigned as higher-order 110 and 210 peaks. On the basis of the position of the 100 peak, the higher-order peak intensities were calculated and marked as arrows in Figure 4. The deviation from the calculated

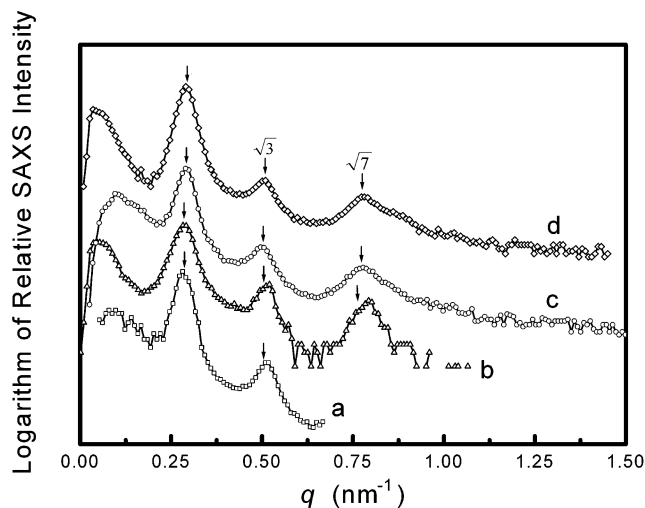


**Figure 4.** One-dimensional equatorial scan data obtained on the two-dimensional SAXS patterns shown in Figure 3: (a) 0 s (unelongated), (b) 20 s ( $\epsilon = 0.2$ ,  $\lambda = 1.2$ ), (c) 90 s ( $\epsilon = 0.9$ ,  $\lambda = 2.5$ ), and (d) 190 s ( $\epsilon = 1.9$ ,  $\lambda = 6.7$ ).

**Table 1. Column Diameter,  $D$ , and Fwhm Determined from the SAXS Data of the SEBS Samples, Collected during the Case 1 Elongation**

Hencky strain, $\epsilon$	column diameter, $D$ (nm)	half-width of the 100 peak (deg in $2\theta$ )
0.0	$11.7 \pm 0.1$	$0.045 \pm 0.003$
0.2	$11.6 \pm 0.1$	$0.047 \pm 0.004$
0.9	$11.4 \pm 0.2$	$0.048 \pm 0.005$
1.9	$11.3 \pm 0.1$	$0.044 \pm 0.003$

peak positions and the broadness of the observed peaks were partly due to the fact that the deformed, elongated specimens were not in a thermodynamic equilibrium.

As shown in Figure 3a–d, the characteristic features remained almost similar, indicating that the initial cylindrical morphology was maintained during the case 1 elongation. On the basis of the position of the 100 peak in Figure 3a–d, the corresponding cylinder diameters,  $D [= 2d_{100}(\sqrt{3}\phi_{PS}/2\pi)^{1/2}]$ , were estimated and summarized in Table 1. Assuming that the 100 peak has a Gaussian profile, the full width at half-maximum (fwhm) in degree was also summarized in this table. Because of the macroscopic strain applied on the sample which caused its scattering centers to deviate from Gaussian statistics, these values contained 7–8% calculation error in the curve-fitting procedures.

On the other hand, Figure 5a–e show the SAXS data of the unelongated and elongated samples subjected in the case 2 elongation, collected at (a) 0 s (unoriented), (b) 20 s ( $\epsilon = 0.2$ ,  $\lambda = 1.2$ ), (c) 70 s ( $\epsilon = 0.7$ ,  $\lambda = 1.9$ ), (d) 200 s ( $\epsilon = 2$ ,  $\lambda = 7.4$ ), and (e) 400 s ( $\epsilon = 4$ ,  $\lambda = 54.6$ ). The elongation direction was along the meridian in these patterns. The corresponding one-dimensional SAXS scans along the peak intensities  $I(q)$  vs scattering vector,  $q$ , were also shown in Figure 6a–e.

In Figure 5a for the unelongated sample, a series of the SAXS peaks appear in the meridional direction, confirming that the PS cylinders of the unelongated samples are initially aligned perpendicular to the stretching direction. As seen in scan a in Figure 6, the most intense peak corresponds to the hexagonal 100 peak and the additional X-ray peaks to the higher-order hexagonal peaks whose  $q$  values are almost in the ratio of  $1:\sqrt{3}:\sqrt{7}$ . Thus, the meridional peaks seen in Figure 5a show that the two-dimensional hexagonal lattice is aligned perpendicular to the stretching direction.

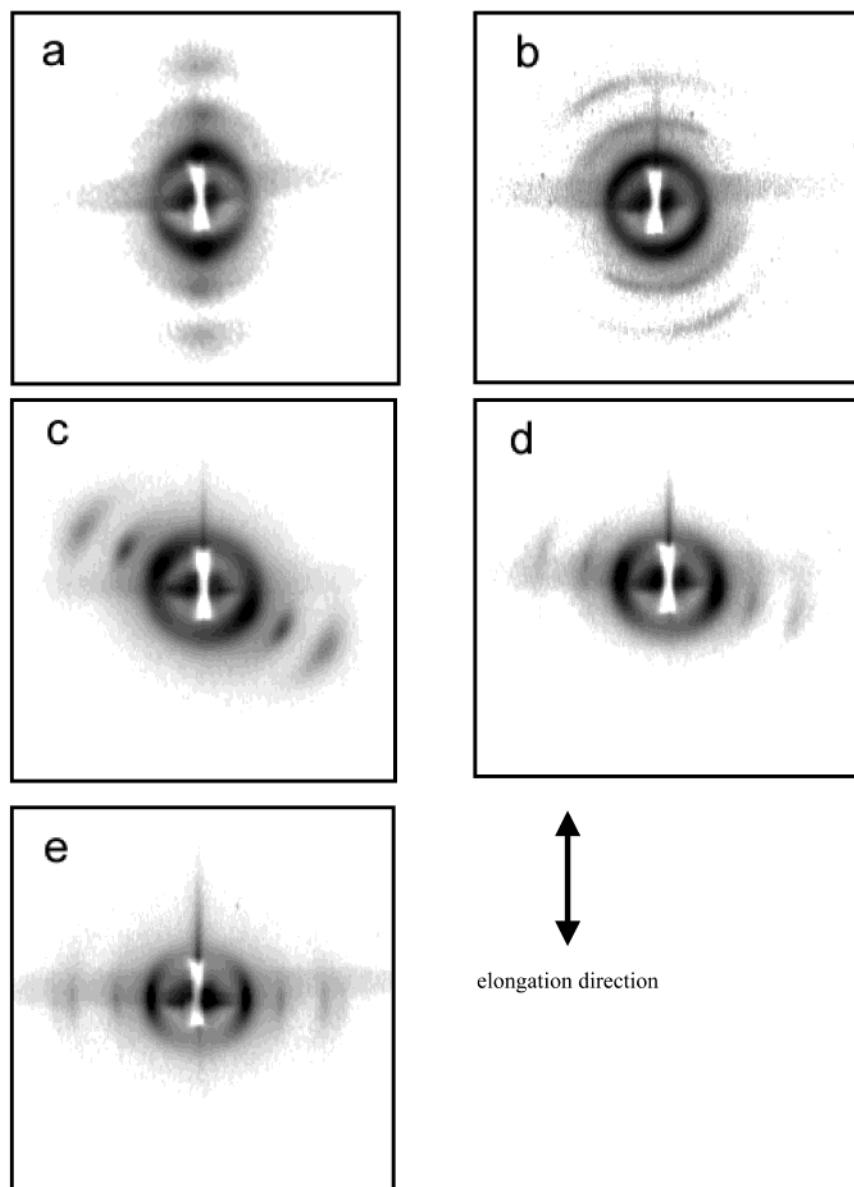


**Figure 5.** Two-dimensional SAXS patterns of the unelongated and elongated samples collected during the case 2 elongation at (a) 0 s (unelongated), (b) 20 s ( $\epsilon = 0.2$ ,  $\lambda = 1.2$ ), (c) 70 s ( $\epsilon = 0.7$ ,  $\lambda = 1.9$ ), (d) 200 s ( $\epsilon = 2$ ,  $\lambda = 7.4$ ), and (e) 400 s ( $\epsilon = 4$ ,  $\lambda = 54.6$ ).

On the basis of the position of the 100 peaks in Figure 6, we estimated the cylinder diameter,  $D$ , during the case 2 elongation and summarized in Table 2. The data show that the measured  $D$  gradually increases at  $\epsilon = 0.2$  (a) and 0.7 (b) but slightly decreases just before their rupture [(d) and (e)]. The initial increase in  $D$  resulted from the increased structural imperfection of the cylinder domains, aligned perpendicularly to the stretching direction. On further elongation near its rupture, the orientation of domains was highly improved, leading to the decrease in  $D$  just before its rupture. The fwhm's of the 100 peaks in Figure 6 were estimated and summarized in Table 2. As seen in the table, it increased due to the increase in structural imperfection during elongation by  $\epsilon = 0.7$ , which was caused by the deformation and rotation of the cylindrical morphology to the stretching direction. On further elongation, it decreased again by the structural reorganization and the further alignment of the deformed cylindrical domains to the stretching direction.

The data scanned along the azimuthal direction provide the information on the rotation of the cylinder

phase during elongation. Figure 7a–e display the data scanned in the azimuthal direction ( $\beta$ ) along the most intense 100 peaks in Figure 5, and  $\beta = 90^\circ$  denotes the meridional direction. The peak intensity at  $\beta = 90^\circ$  in Figure 7a reveals that the cylinders of the unelongated sample are preferentially aligned in the direction perpendicular to the stretching direction. Figure 7b for the sample at  $\epsilon = 0.2$  shows that the main peak intensity has moved to  $\beta$  of approximately  $108^\circ$ . An additional weak peak is also found at around  $157^\circ$ . The broadness and existence of two peaks in the azimuthal scan profile may be caused by the rotation of the grains that are preferentially aligned in two different directions. In each grain, the PS cylinders are aligned along the preferred direction.

Figure 7c for the sample at  $\epsilon = 0.7$  shows the peak at approximately  $60^\circ$  from the meridian, and the peak width is smaller than that for  $\epsilon = 0.2$ . The scan profile indicates that most cylinders are uniformly inclined by approximately  $30^\circ$  to the elongation direction. The absence of the four-point pattern indicates that the cylinder phase of the case 2 samples is preferentially

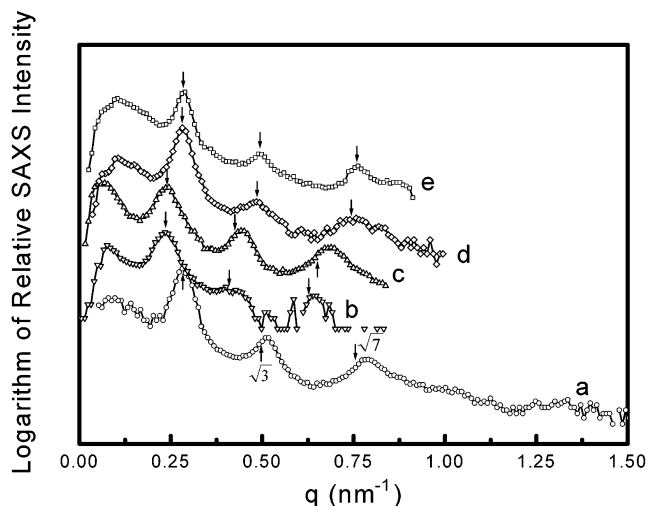


**Figure 6.** One-dimensional scan data obtained on the two-dimensional SAXS patterns shown in Figure 3: (a) 0 s (unelongated), (b) 20 s ( $\epsilon = 0.2$ ,  $\lambda = 1.2$ ), (c) 70 s ( $\epsilon = 0.7$ ,  $\lambda = 1.9$ ), (d) 200 s ( $\epsilon = 2$ ,  $\lambda = 7.4$ ), and (e) 400 s ( $\epsilon = 4$ ,  $\lambda = 54.6$ ).

**Table 2. Column Diameter,  $D$ , and Fwhm Determined from the SAXS Data of the SEBS Samples, Collected during the Case 2 Elongation**

Hencky strain, $\epsilon$	column diameter, $D$ (nm)	half-width of the 100 peak (deg in $2\theta$ )
0.0	$11.6 \pm 0.1$	$0.042 \pm 0.003$
0.2	$13.5 \pm 0.2$	$0.049 \pm 0.003$
0.7	$13.7 \pm 0.2$	$0.061 \pm 0.005$
2.0	$11.6 \pm 0.1$	$0.045 \pm 0.004$
4.0	$11.4 \pm 0.1$	$0.034 \pm 0.003$

tilted to the stretching direction. A similar morphology was previously reported.<sup>5</sup> In Figure 7d,e, the 100 peak is found at around  $180^\circ$ , almost on the equator, indicating that the initial perpendicular cylinder domains have been rotated by approximately  $90^\circ$ , parallel to the elongation direction. In addition, the disappearance of the amorphous halo also points out that the global alignment of the cylindrical domains to the stretching direction has been achieved.

The degree of orientation of the cylindrical domains can be quantitatively expressed by order parameter,  $f$ , defined by the following equation:

$$f \equiv \frac{3\langle \cos^2 \beta \rangle - 1}{2} = \frac{\int I(\beta) |\sin \beta| \left( \frac{3}{2} \cos^2 \beta - \frac{1}{2} \right) d\beta}{\int I(\beta) |\sin \beta| d\beta} \quad (5)$$

where  $\langle \cos^2 \beta \rangle$  is the mean-square cosine of the angle between cylinder axis and the elongation axis;  $I(\beta)$  is the azimuthal intensity distribution corresponding to the peak widening due to misorientation. Optical birefringence, infrared dichroism, nuclear magnetic resonance, and X-ray scattering are among the most popular methods used to measure molecular order with different characteristics. Since X-ray scattering techniques are effective in characterizing the orientation of molecules and domains separately, we employ it to examine the orientation of the cylindrical domains and its change during case 2 elongation. On the basis of the azimuthal scan data along the first-order peak shown in Figure 7, the  $f$ s at different levels of Hencky strains were estimated by eq 5 and plotted in Figure 8. Since the amorphous halo at the same diffraction angle was almost absent, the correction of the background scat-

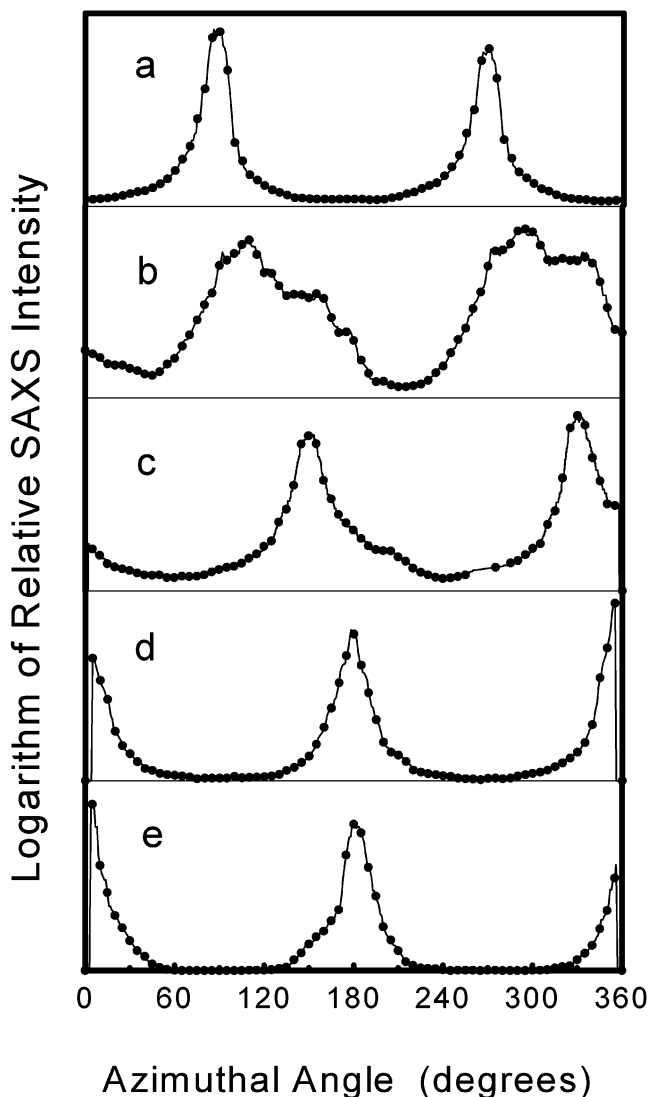


**Figure 7.** Azimuthally scanned data along the strongest 100 peak in Figure 6: (a) 0 s (unoriented), (b) 20 s ( $\epsilon = 0.2$ ,  $\lambda = 1.2$ ), (c) 70 s ( $\epsilon = 0.7$ ,  $\lambda = 1.9$ ), (d) 200 s ( $\epsilon = 2$ ,  $\lambda = 7.4$ ), and (e) 400 s ( $\epsilon = 4$ ,  $\lambda = 54.6$ ).

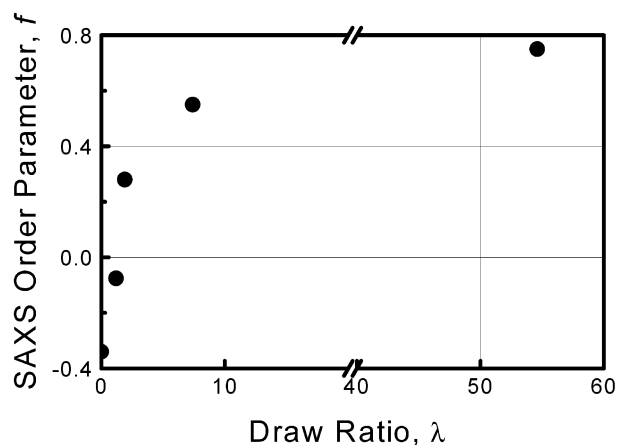


**Figure 8.** Plot of order parameter,  $f$ , vs Hencky strain determined from the azimuthal intensity distribution along the 100 peak in Figure 5.

tering from the observed 100 peak intensity was ignored in the calculation.

In Figure 8, we see that the  $f$  for the orientation of the cylinder domains increases rapidly as the elongation

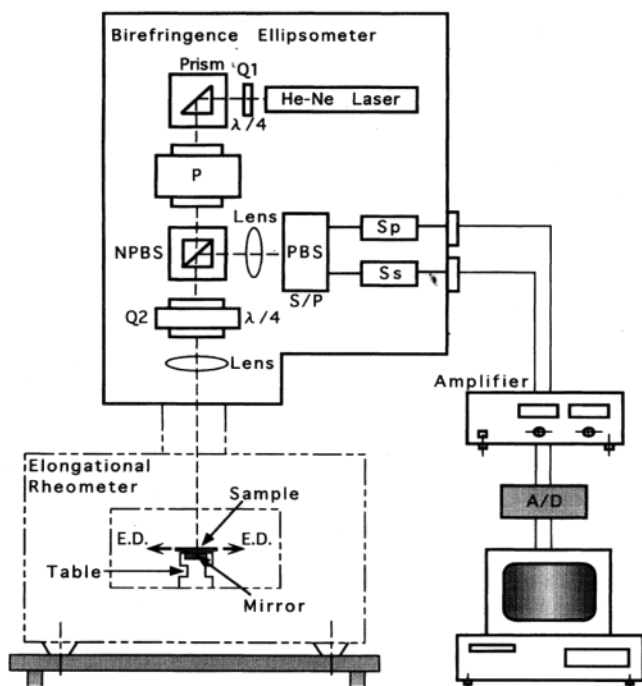


**Figure 9.** Schematic diagram of the birefringence optical system in our EFOR apparatus.

proceeds up to near  $\lambda \approx 2$  ( $\epsilon \approx 0.7$ ), indicating that the development of the ordering due to the realignment or rearrangement process of the cylindrical domains is significant in the early stage of elongation. Beyond  $\lambda \approx 2$ , it continues to increase, but less rapidly, by further alignment of the cylinders into the stretching direction.

## Discussion

**Morphological Change at Small Strains.** The elongational flow-induced deformation behavior of both the perpendicular and the parallel cylindrical phase has been investigated at various stages of elongation. The data point out that the morphological evolution of the cylindrical phase depends on the initial orientation of the cylinders before elongation. At small strains, either the PS or the PEB domain was preferentially elongated depending on their geometrical arrangement to the elongation direction. The retardation,  $R(t)$ , provides information on the molecular orientation at small strains. In our EFOR system, as shown in Figure 9, the He-Ne laser light at 632 nm from the source was once circularly polarized with polarizer and a quarter wave ( $\lambda/4$ ) Q1 plate before entering into the total reflecting prism and converted back with the polarizer P to a plane-polarized light with electric vector at  $0^\circ$  relative to the direction of elongation.<sup>22</sup> The plane-polarized light was incident on another quarter wave Q2 plate set at  $45^\circ$  to the direction of elongation and passed through the specimen under elongation. After passing through the specimen, the elliptically polarized light was reflected back by the mirror. Then it passed the specimen and Q2 plate again and deflected by  $90^\circ$  with the half mirror at nonpolarizing beam splitter (NPBS) and reached the polarizing beam splitter (PBS) set at  $45^\circ$ . Then the beam was split and detected at a silicon photoelectric detector  $S_p$  at  $45^\circ$  inclination and with another detector  $S_s$  at  $-45^\circ$  inclination so that the intensities  $DP$  and  $DS$ , perpendicular and parallel to the stretch direction, respectively, were detected with

$S_p$  and  $S_s$  detectors. The retardation,  $R(t)$ , can be expressed by the phase difference  $\Delta t$  at time  $t$  between the polarized lights on the detectors, with intensities  $DS$  and  $DP$ :

$$R(t) = \frac{DS - DP}{DS + DP} = \sin[2\Delta(t)] \quad (6)$$

Experimentally, the phase difference  $\Delta(t)$  is determined by the apparent retardation  $R_{app}(t)$  and measured intensities,  $DS_a$  ( $DS + D_0$ , where  $D_0$  is the unpolarized background) and  $DP_a$  ( $DS + D_0$ ) and on the detectors:

$$R_{app}(t) = \frac{DS_a - DP_a}{DS_a + DP_a} = \frac{DS - DP}{DS + DP + 2D_0} = A_m \sin[2\Delta(t)] \quad (7)$$

where  $A_m [= (DP + DS)/(DP + DS + 2D_0)]$  denotes the amplitude factor. To eliminate the effect of the preexisting alignment of the cylinders in the unoriented specimens, the initial difference between the intensities  $DP_a$  and  $DS_a$  was offset in the beginning of each EFOR measurement. The quantity we wish to determine is the overall phase difference  $\Delta(t)$  that can be obtained from the true retardation  $R(t)$ . The phase difference  $\delta(t)$  per a single layer of the specimen at a time  $t$  between the consecutive minimum/maximum is defined as

$$\delta(t) = \arcsin [R(t)]/2 \quad (8)$$

where  $R(t) = [1 + (D_0/4)]R_{app}(t)$  with the factor  $[1 + (D_0/4)]$  being given from the neighboring peak-to-peak difference. We then calculate the overall phase difference  $\Delta(t)$  at time  $t$  as

$$\Delta(t) = \delta(t) + [(\pi/4) + \pi(m - 1)/2] \quad (9)$$

where  $m$  is the number of maximum/minimum peaks of  $R_{app}(t)$  appearing by the time  $t$ . Then if the sample thickness at time  $t$  is  $d(t)$ , we determine the value of birefringence  $\Delta n(t)$  as

$$\Delta n(t) = \lambda_{\text{He-Ne}} \Delta(t) / 2\pi d(t) \quad (10)$$

The  $R_{app}(t)$  measured during the elongation of the PS melt started with a negative value, indicating that PS has a negative birefringence, whereas one from low-density polyethylene exhibited a positive value in the beginning of elongation.<sup>26,27</sup>

Parts a and b of Figure 10 show the apparent retardation data measured during the case 1 and 2 elongation, respectively. By approximately 5.5 s,  $R_{app}(t)$  could not be measured due to the idle time of the EFOR equipment. In parts a and b of Figure 10, the initial  $R_{app}(t)$ 's before about 20 s show positive and negative values in the case 1 and 2 elongation, respectively. The results suggest that the deformations at small strains in the case 1 and 2 elongations are mainly determined by the deformation of the PS and PEB domain, respectively.

The cylinder morphology may not be much changed during the case 1 elongation because of the relatively rigid PS domains, aligned parallel to the elongation direction. On the other hand, in the case 2 elongation, the increase in  $\eta_E(\dot{\epsilon}_0; t)$  is attributed to the deformation of the soft PEB domains, which eventually causes the fragmentation and reorganization of the domain as well as the grain structures along the stretching direction.

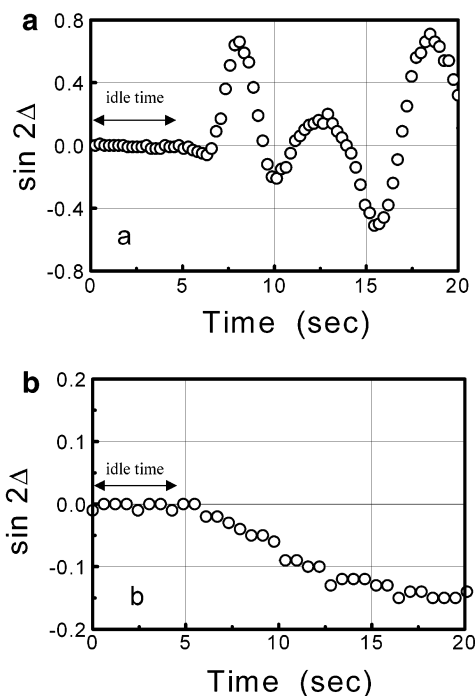


**Figure 10.** Plots of apparent retardation,  $\sin[2\Delta(t)]$ , vs time measured during the (a) case 1 and (b) case 2 elongation.

### Morphological Change at Large Deformation:

**Case 1 Elongation.** With increasing strain up to  $\epsilon = 0.9$ , the measured  $\eta_E(\dot{\epsilon}_0; t)$  in the case 1 elongation slightly decreases to reach almost a steady state before rupture. The corresponding SAXS data of the samples collected at  $\epsilon = 0.9$  show almost the same feature as those seen in the unelongated sample, indicating that the parallel cylinder alignment persisted up to the rupture. The fact that the 100 peak is broader at this stage of elongation indicates that the packing order of the PS cylinders is poor due to large strains applied. The result points out that the case 1 elongation by  $\epsilon = 0.9$  causes the misaligned cylinders to be aligned to the stretching direction.

At  $\epsilon = 1.9$ , the sharpness of the 100 peak and its shift to the wide angle region could be due to the reorganization and realignment of the domains or molecules beyond yielding. The absence of the amorphous halo in the SAXS pattern also indicates that the disordered phase is converted into the order phase at higher elongation. The improved cylinder alignment into the stretching direction may be associated with the better packing and the structural ordering of the highly elongated cylindrical phase. The persistence of the characteristics seen in Figure 3a–d also indicates that the initial cylindrical morphology is maintained almost up to rupture.

**Case 2 Elongation.** At intermediate amount of strain ( $0.2 < \epsilon \leq 0.7$ ) during the case 2 elongation, the  $\eta_E(\dot{\epsilon}_0; t)$  value is slightly decreased to be almost the steady state. Figure 5b,c shows that the cylinder domains gradually rotate into the stretching direction, and at  $\epsilon = 0.7$ , the cylinder axes were globally inclined by approximately  $30^\circ$  to the stretching direction. In Figure 5b,c additional peaks did not appear during elongation. In the corresponding one-dimensional SAXS scan data (b) in Figure 6, the scattering vector  $q$  value of the peaks gradually moves to the small angle region on increasing strain by  $\epsilon = 0.2$ . The result is probably

due to the increased structural imperfection that may be attributed to a deformation of the PEB matrix, resulting in larger cylinder-to-cylinder distances and the disruption of the perpendicularly aligned domain structure. At  $\epsilon = 0.7$  shown in the plot c of Figure 5, we see the cylindrical domains, inclined to the stretching direction by approximately  $30^\circ$ . The absence of the four-point pattern, indicative of the absence of the “chevron” morphology,<sup>28</sup> is probably due to the initial alignment of the domains which is not exactly perpendicular to the elongation direction and causes the domains to rotate in either one of the two possible directions. The peak width in the  $2\theta$  direction becomes broader due to the decreased packing order of the cylinders, induced by the rotation of the domains.

On further elongation beyond  $\epsilon = 0.7$ , the  $\eta_E(\dot{\epsilon}_0; t)$  begins to rapidly increase further up to the rupture and displays the strong strain-induced hardening behavior. In Figure 5c, we see the peak in the  $2\theta$  direction is slightly sharper due to the increase of grain size along with the improved packing order of the cylinders at large deformation. The SAXS data show a series of equatorial X-ray peaks, confirming the rotation of the cylinders from the perpendicular to the parallel alignment. The parallel alignment of the cylinders was achieved relatively easily at high temperature where the molecular correlation became weaker by the increased thermal motion of molecules than at low temperatures. The domains composed of the associated, mobile molecules, confined by their interfaces seem to rotate further to the stretching direction. A similar result was found during shearing of the diblock copolymers, showing that a large amount of shear produced the parallel or perpendicular alignment of lamellar domains where the domain interfaces were aligned to the shearing direction.<sup>8–13</sup>

### Conclusions

The combination of the EFOR and SAXS measurements provided the information on the structural evolution of the cylindrical domains under elongation. The deformation behavior varied with the initial alignment of the cylinder domains. The case 1 elongation induced the preferential elongation of the relatively rigid PS domains in the beginning of elongation and the initial parallel morphology largely persisted at large deformation up to rupture. The reorganization of the grain structure along with yielding of the PS domains decreased the  $\eta_E(\dot{\epsilon}_0; t)$  beyond the yielding point during the case 1 elongation.

On the other hand, for the case 2 elongation, the soft PEB matrix was preferentially aligned in early stage of elongation. The further elongation during the case 2 elongation caused the deformation, rotation, and fragmentation of the grain structure along the stretching direction, resulting in a decrease in the  $\eta_E(\dot{\epsilon}_0; t)$  values in the range of  $0.2 < \epsilon \leq 0.7$ . The rapid increase of the  $\eta_E(\dot{\epsilon}_0; t)$  in the later stage, exhibiting the strain-induced hardening behavior, was caused by the realignment of the domain structure. Moreover, the decrease of the width of the 100 peak resulted from the reformation and growth of the grains along with the molecular and domain orientation. The SAXS and EFOR measurements indicated that the elongation behavior of the cylinder microdomain at high temperatures was mostly governed by the morphological evolution of the cylinder domain and the rearrangement process of the grain

structure during elongation, especially in the case 2 elongation.

**Acknowledgment.** The authors thank Mr. I. Yonezawa of Asahi Chemical Co. for his valuable assistance for providing the roll-processed films in our study. This work was supported by the Japanese Ministry of Education, under the project of Future Data Storage Materials, and the Academic Frontier Center at the Toyota Technological Institute.

### References and Notes

- (1) Okamoto, M.; Kojima, A.; Kotaka, T. *Polymer* **1997**, *39*, 2149.
- (2) Kano, Y.; Okamoto, M.; Kotaka, T. *Polymer* **1999**, *40*, 2459.
- (3) Kim, Y. H.; Okamoto, M.; Kotaka, T.; Ougizawa, T.; Tchiba, T.; Inoue, T. *Polymer* **2000**, *41*, 4747.
- (4) Takahashi, T.; Toda, H.; Minagawa, K.; Takimoto, J.-I.; Iwakura, K.; Koyama, K. *J. Appl. Polym. Sci.* **1995**, *56*, 411.
- (5) Kotaka, T.; Okamoto, M.; Kojima, A.; Kwon, Y. K.; Nojima, S. *Polymer* **2001**, *42*, 1207. Kotaka, T.; Okamoto, M.; Kojima, A.; Kwon, Y. K.; Nojima, S. *Polymer* **2001**, *42*, 3223.
- (6) See, for example: Hamley, I. W. Melt Phase Behaviour of Block Copolymers. In *The Physics of Block Copolymers*; Oxford University Press: New York, 1998.
- (7) Winey, K. I.; Patel, S. S.; Larson, R. G.; Watanabe, H. *Macromolecules* **1993**, *26*, 2542.
- (8) Polis, D. L.; Winey, K. I. *Macromolecules* **1998**, *31*, 3617.
- (9) Okamoto, S.; Saijo, K.; Hashimoto, T. *Macromolecules* **1994**, *27*, 5547.
- (10) Zhang, Y.; Wiesner, U.; Spiess, H. W. *Macromolecules* **1995**, *28*, 778.
- (11) Gupta, V. K.; Krishnamoorti, R.; Chen, Z.-R.; Kornfield, J. A. *Macromolecules* **1996**, *29*, 875.
- (12) Gupta, V. K.; Krishnamoorti, R.; Chen, Z.-R.; Kornfield, J. A.; Smith, S. D. *Macromolecules* **1996**, *29*, 1359.
- (13) Chen, Z. R.; Issaian, A. M.; Kornfield, J. A.; Smith, S. D.; Grothaus, J. T.; Satkowski, M. M. *Macromolecules* **1997**, *30*, 7096.
- (14) Keller, A.; Redemonte, E.; Willmouth, F. M. *Nature (London)* **1970**, *225*, 538; *Kolloid Z. Z. Polym.* **1970**, *238*, 385.
- (15) Fujumura, M.; Hashimoto, T.; Kawai, H. *Rubber Chem. Technol.* **1978**, *51*, 215.
- (16) Kawai, H.; Hashimoto, T. *J. Macromol. Sci.* **1980**, *B17*, 427.
- (17) Seguela, R.; Prudhomme, J. *Macromolecules* **1981**, *14*, 197.
- (18) Pakula, T.; Saijo, K.; Kawai, H.; Hashimoto, T. *Macromolecules* **1985**, *18*, 7096.
- (19) Yamaoka, I.; Kimura, M. *Polymer* **1993**, *34*, 4399.
- (20) Cohen, Y.; Albalak, R. J.; Dair, B. J.; Capel, M. S.; Thomas, E. L. *Macromolecules* **2000**, *33*, 6502.
- (21) Meissner, J.; Hostettler, J. *Rheol. Acta* **1994**, *33*, 1.
- (22) Kotaka, T.; Kojima, A.; Okamoto, M. *Rheol. Acta* **1997**, *36*, 646.
- (23) Kobori, Y.; Kwon, Y. K.; Okamoto, M.; Kotaka, T. Manuscript in preparation.
- (24) Rudd, J. F. Physical Constants of Polystyrene. In *Polymer Handbook*, 3rd ed.; Brandrup, J., Immergut, E. H., Eds.; John Wiley & Sons: New York, 1989.
- (25) Gubler, X.; Kovacs, X. *J. Polym. Sci.* **1959**, *34*, 551.
- (26) Janeschitz-Kriegl, H. In *Polymer Melt Rheology and Flow Birefringence*; Springer-Verlag: Berlin, 1983.
- (27) White, J. L. In *Principles of Polymeric Engineering Rheology*; Wiley: New York, 1990.
- (28) Honeker, C. C.; Thomas, E. L. *Chem. Mater.* **1996**, *8*, 1702.

MA020503K